ICARUS 89, 113–121 (1991)

# Coagulation of Particles in Saturn's Rings: Measurements of the Cohesive Force of Water Frost

A. P. HATZES,[1,*,†] F. BRIDGES,[‡] D. N. C. LIN,[*] AND S. SACHTJEN[‡]

*Board of Studies in Astronomy and Astrophysics and ‡Board of Studies in Physics, University of California, Santa Cruz, California 95064, and †McDonald Observatory, University of Texas, Austin, Texas 78712-1083*

Received December 4, 1989; revised June 29, 1990

**The cohesive properties of water ice particles may play an important role in the dynamics of ring particles as well as in the evolution of the particle size distribution. In this paper we present preliminary experimental data on the sticking force of water ice particles. The data indicate that the sticking force between smooth, frost-free ice particles is less than a dyne; however, the presence of a layer of water frost 10–100 $\mu$m thick on the ice surfaces increases this force up to 100 dyn. The resulting sticking force is dependent on the impact velocity of the particle and is maximized for some intermediate ($\sim$0.1 cm sec$^{-1}$) velocity. Consequently, a "Velcro" model is presented to describe the surface structure responsible for the sticking. The data indicate that there is a critical impact velocity of order 0.03 cm sec$^{-1}$ below which cohesion of particles always occurs. After sticking, the ice particle undergoes a damped harmonic motion characteristic of a linear force law having a range of order 10 $\mu$m. A spring constant of $k \approx 10^4$ dyn/cm is derived. We show that given the optical depth of micrometer-sized grains in Saturn's rings, particles are most likely coated with a significant layer of frost such that the cohesion of particles may be an important process in ring dynamics. Finally using the largest measured sticking forces we estimate the largest aggregate of ice particles capable of surviving tidal disruption to be about 10 m.** 

## I. INTRODUCTION

The key to understanding the observed macroscopic properties of the planetary rings may lie in the collisional properties of the constituent ring particles (Maxwell 1859, Jeffreys 1947). For instance Goldreich and Tremaine (1978) showed that the velocity dispersion of the ring particles as well as the ring thickness is determined by the coefficient of restitution of the ring particles. Such quantities as the energy loss during ring particle collisions, the mass transferred between particles during a collision, and the sticking probability as well as the corresponding cohesive force may provide fundamental information toward our understanding of ring particle dynamics.

In an attempt to simulate collisions between planetary-ring particles, we have carried out a series of controlled laboratory experiments. The surfaces of the ring particles are composed primarily of water ice (Pilcher *et al.* 1970) although non-ice material such as silicates could contribute a significant fraction of the total composition (Cuzzi *et al.* 1980). In our experiments we determine the various collisional properties of water ice at impact velocities and in an environment pertinent to planetary rings. First, we determined the velocity dependence of the coefficient of restitution, $\varepsilon(v)$. Based on a simple model for ring particle collisions (Goldreich and Tremaine 1978), the experimentally determined values of $\varepsilon(v)$ yielded a velocity dispersion $\sim$0.1 cm sec$^{-1}$ for the ring particles and resulting estimates for the ring's thickness consistent with Voyager's data for Saturn's rings (Bridges *et al.* 1984). Further and more extensive experiments revealed that $\varepsilon(v)$ was dependent on the surface characteristics of the colliding particles. Collisions of ice spheres with roughened surfaces or those covered with a frosty layer were more dissipative by 30–50% over smooth spheres (Hatzes *et al.* 1988, hereafter Paper I). However, repeated collisions of frosted ice spheres rapidly compacted the soft contact surface. The resulting asymptotic value for $\varepsilon$ approached that for a clean, smooth ice sphere after 5–10 collisions made at impact velocities of order 0.1 cm sec$^{-1}$. A similar result was obtained for ice spheres which had finely fractured surfaces.

The collisional energy dissipation can be attributed to both deformation in the contact area and mass transfer between ice spheres (McDonald *et al.* 1989). The amount of mass being transferred during each collision is comparable to that contained in the compressed volume in the contact region. For particles with smooth surfaces, the experimentally determined compressed volume is compa-

[1] Current address: Astronomy Department, RLM 15.308, University of Texas, Austin, TX 78712-1083.



0019-1035/91 $3.00

rable with that predicted by the Hertz theory (Borderies *et al.* 1984), although ice spheres with rough surfaces can have a mass transfer an order of magnitude larger than is predicted by this theory.

Another important collisional property of water ice with potential implications to ring dynamics is the probability that ice particles stick. Collisionally induced cohesion is one process by which small particles may coagulate and large particles may grow in size. If the sticking probability for relevant collisional velocities is sufficiently large, the cohesive force between the coagulated particles could be as important as the particles' self gravity in binding an aggregate of small particles to form "dynamical ephemeral bodies" (DEBs) (Weidenschilling *et al.* 1984). The magnitude of the sticking force also should determine the limiting size of an aggregate of particles that can exist without tidal disruption by the planet. To investigate the sticking probability and cohesion strength, a new series of experiments were undertaken; the results are reported in this paper.

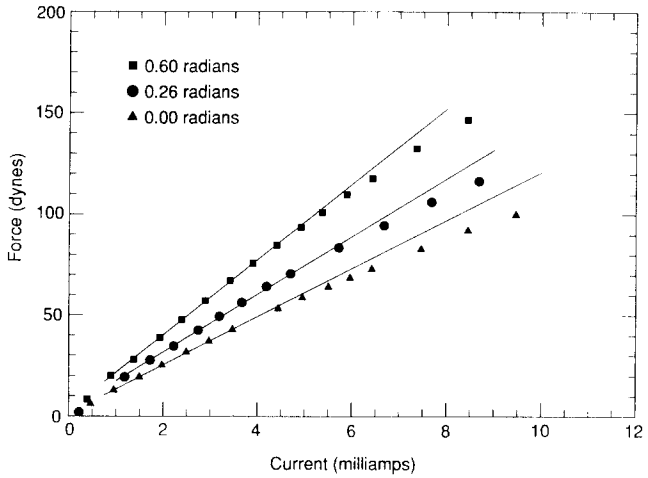


FIG. 1. A typical calibration curve relating the solenoid current to the actual force applied to the disk pendulum for three initial equilibrium positions of the pendulum. When the pendulum is displaced by 0.26 and 0.60 radians the bar magnet on the disk penetrates deeper into the solenoid coil where it encounters a larger magnetic field, thus resulting in a steeper $F(i)$ relationship. Note the departure from linearity for large current values and thus larger displacements of the disk pendulum.

## II. EXPERIMENTAL PROCEDURE

These experiments were performed using the same experimental apparatus described in Paper I. Briefly, it consists of an ice sphere attached to a disk pendulum that can be made to oscillate at periods of up to 60 sec. A movable ice brick is positioned such that the ice sphere strikes the brick when the pendulum has its maximum angular velocity. The position of the ice sphere is accurately measured during each collision using a capacitive displacement device (CaDD) whose output voltage is linearly related to the displacement of the pendulum. The CaDD is capable of measuring the time-dependent displacement of the ice sphere during a collision to within 0.1 $\mu$m. A detailed description of the apparatus as well as the operation of the CaDD is given in Paper I.

For the cohesion measurements the pendulum is allowed to come to rest in its equilibrium position. The ice brick platform is slowly raised until it makes nominal contact with the ice sphere. Mounted at the bottom of the disk pendulum is a small bar magnet which rests inside a solenoid when the pendulum is in its equilibrium position (see Fig. 1 of Paper I). A displacement of the pendulum is initiated by applying a pulse of current through the solenoid that creates a magnetic field of polarity opposite to that of the pendulum's magnet. The resulting torque applied to the freely swinging pendulum causes a displacement of the pendulum whose magnitude can be varied by changing the amount or duration of the flow of current through the solenoid.

When a collision results in the ice sphere bonding to the ice brick surface, we measure the sticking force as follows. A current is applied to the solenoid to move the ice ball away from the ice brick. The current is slowly increased until the ball and brick separate. The current at the breaking point provides a measure of the sticking force. The calibration of current versus force depends on the position of the pendulum at contact. Typical calibration curves are shown in Fig. 1.

## III. STICKING MEASUREMENTS

Qualitatively, the sticking probability and cohesive force are a sensitive function of the surface structure of the ice sphere. At low impact velocities, ~0.01 cm sec$^{-1}$ collisions between a smooth, frost-free sphere and brick do not lead to sticking as the cohesive force between the sphere and the brick is negligibly small, below the detectability of this experiment (<1 dyn). However, with a comparable impact velocity, the sticking probability and cohesive force increase significantly by the presence of a frost layer 10–100 $\mu$m thick. This frost layer was deposited by a gas-handling system which allowed water-saturated nitrogen gas to blow past the contact surface of the brick and sphere. This frosting was performed at temperatures ranging from 90 to 150°K and at pressures of no more than a few Torr. For such frosted conditions the sticking force ranged from a few dynes to 100 dyn.

To demonstrate this property, a series of experiments was carried out in which an ice sphere of radius 2.5 cm was prepared with a ~30 to 50-$\mu$m layer of water frost deposited on its surface. On the first collision, the ice sphere and the brick stuck together. The force required

to pull the ice sphere from the brick was measured. A subsequent low-velocity collision was made keeping the position of the ice brick and consequently the position of the contact point on the sphere fixed. Once again, the collision led to cohesion. This procedure was repeated several times using the same impact velocity, typically $V_{\text{impact}} \sim 0.1$ cm sec$^{-1}$.

In Fig. 2, the sticking force is shown as a function of collision number for such a typical experimental run. (Many runs have actually been carried out.) The sticking force from the first collision is approximately 100 dyn while for the second one it dramatically dropped to 33 dyn. For subsequent collisions the sticking force monotonically decreased from 30–40 to 5 dyn by the seventh or eighth collision. The sticking forces in all our runs vary between 1 and 150 dyn and always decrease with the number of collisions. These results suggest that the surface structure responsible for the sticking force is being damaged by repeated collisions.

The sticking force resulting from the sixth collision in Fig. 2 deviates from the monotonically decreasing trend. This collision was aberrant in that the impact velocity was at least twice as large as in the other collisions and consequently the sticking force was two to three times as large as that expected from the subsequent trend of sticking force versus collision number. In this case the higher-velocity impact would serve to press the two layers closer together, possibly resulting in a stronger bond strength. In a second series of experiments, the impact velocity prior to sticking was measured more accurately. For this series, the ice sphere was prepared in the same manner as above and the results are shown in Fig. 3. The first four collisions of the ice sphere with the brick with measurable sticking forces were made with an impact velocity < 0.02

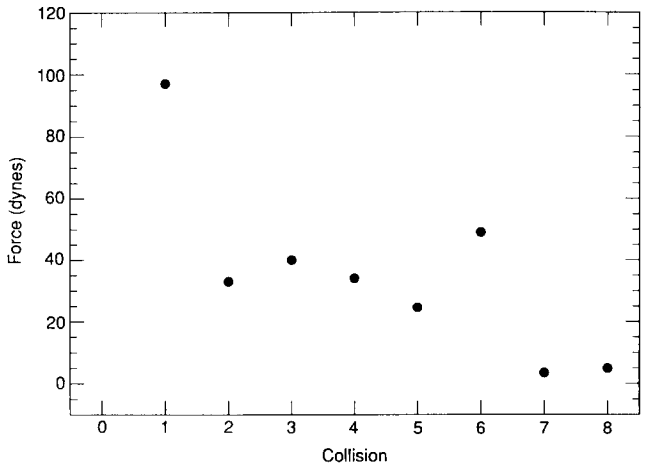


FIG. 2. Sticking force as a function of collision number for an ice sphere of 2.5-cm radius of curvature and with a frost layer approximately 30–50 $\mu$m thick.

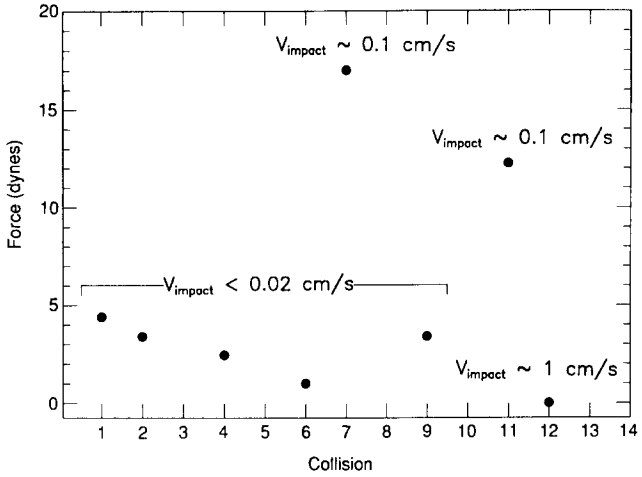


FIG. 3. Sticking force as a function of collision number for an ice sphere of 2.5-cm radius of curvature and with a frost layer approximately 30–50 $\mu$m thick. In this instance the impact velocity prior to sticking was measured. Missing collisions are those for which sticking occurred but for which an accurate measurement of the force was not obtained.

cm sec$^{-1}$. The measured force for these collisions monotonically decreased from about 5 dyn to approximately 1 dyn. A decrease in the sticking force with repeated impacts once again suggests compaction of the frost with each collision. The missing collisions in Fig. 3 were incidents for which a sticking collision occurred but for which sticking measurements were not made in this particular run due to complications in the data taking process.

The ice sphere was then impacted with the brick at an intermediate velocity of 0.1 cm sec$^{-1}$ (collision 7), resulting in a higher sticking force of 17 dyn, or ~17 times higher than the previously measured value. The next collision was made with an impact velocity comparable to that of the first collisions (0.02 cm sec$^{-1}$) and resulting in a sticking force consistent with the first measurements (3 dyn). For collision 11 the impact velocity was 0.1 cm sec$^{-1}$ and once again the sticking force (12 dyn) was comparable to the previous value for comparable impact velocity. Finally, high-velocity ($V_{\text{impact}} \sim 1$–2 cm sec$^{-1}$) impacts were imposed and the collisions were no longer cohesive. The high-velocity impacts may have pulverized the surface frost and compressed the contact region so that the ice sphere retained an effectively smooth surface. Following these collisions we were unable to make the ice sphere stick to the brick even at impact velocities comparable to those previous collisions for which sticking occurred. This places an upper limit of less than a dyne for the sticking force for these collisions.

## IV. A MODEL FOR THE SURFACE STRUCTURE

Figure 3 can be used to provide a qualitative description of the structure of the surface frost responsible for the

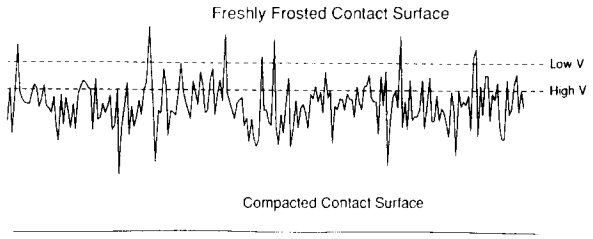


FIG. 4. The "Velcro" model for the surface structure responsible for sticking. (Top) A freshly frosted ice particle results in a rough surface with many jagged peaks. An impact at low velocity results in a shallow penetration (top dashed line) of the two layers and in a rather low sticking force. A higher impact velocity results in a deeper penetration (lower dashed line) and as a result the peaks can better grasp the adjacent layer. (Bottom) After several high-impact velocities the surface layer is pulverized and consequently it loses its grasping ability. The resulting sticking force is negligible.

cohesion of the ice particles. Any such description must be able to account for the three pertinent features of Fig. 3: (1) a monotonic decrease of the resulting sticking force for repeated collisions made at the same impact velocity; (2) a maximization of the sticking force for intermediate impact velocities ($V_{\text{impact}} \sim 0.1$ cm sec$^{-1}$); and (3) the absence of any sticking collision even at low impact velocities after several high-velocity impacts ($V_{\text{impact}} \sim 1$–2 cm sec$^{-1}$).

One possible interpretation of the experimental data is that the surface of the ice sphere becomes relatively rough as frost microparticles are deposited onto the ice sphere. In Fig. 4, we qualitatively characterize the surface structure as having many protruding "peaks" and "valleys." At low impact velocities there is insufficient energy to drive these protrusions into the frost layer of the adjacent particle. This is marked by the upper dashed line in the figure that indicates the depth of penetration for a low-velocity impact. As a result the contact area between the two particles is greatly diminished and a relatively low cohesive force results.

Collision at a slightly higher velocity (~0.1 cm sec$^{-1}$) results in larger cohesive force because the larger kinetic energy of the ice sphere drives the jagged protrusions deeper into the adjacent frost layer. The deformed and dislocated peaks from both the sphere and the brick are interlocked to provide a stronger bond. Deeper penetration also increases the contact area between the two surfaces which should also result in an increased cohesive force. Figure 3 indicates that the sticking force measured after two modest velocity impacts ($V_{\text{impact}} \sim 0.1$ cm sec$^{-1}$) is largely the same in spite of the fact that the ice sphere has undergone several low-velocity impacts in the interim. This suggests that the rough surface of the ice sphere is maintaining its integrity after a sticking collision. The two frost surfaces may even be self-molding, that is, the surface microchips may jostle about such that a "peak" from one surface finds its way into the "valley" of the other surface. This would result in the maximization of the contact area between the two surfaces as well as provide a natural interlocking mechanism. Again this should result in an increased sticking force. Also, as the two particles are pulled apart, microchips may be pulled and displaced from their position on the surface, thus rejuvenating the "jaggedness" of the contact area and thereby maintaining the cohesive properties of the particles.

Finally, when the ice sphere is collided at larger impact velocities (1–2 cm sec$^{-1}$) there is sufficient energy to pulverize the protruding peaks, resulting in a relatively smooth, compacted frost surface as illustrated in the lower part of Fig. 4. Deprived of its jagged features the frost layer loses its interlocking property. We speculate that the interlocking effect rather than chemical bonds between the two layers provides the primary mechanism for cohesion, since chemical bonding should not be affected by the pulverization of the contact surface at high impact velocities. The total contact area on the atomic scale between the case of smooth and roughened surfaces is unlikely to differ by many orders of magnitude which would be required to produce the observed sticking forces. This interlocking effect produced by the surface protrusions of the water frost is reminiscent of the effect produced by the popular commercial material Velcro. For this reason we refer to the scenario just described as the "Velcro" model for sticking of frost-ladened ice spheres.

## V. COHESIVE PROPERTIES OF THE CONTACT REGION

### *Evidence for a Critical Velocity for Sticking*

Because the CaDD enables us to accurately measure the position of an ice sphere as a function of time during the collisions, the evolution of a nonsticking and sticking collision can be examined in detail. An ice sphere with a radius of 2.5 cm was coated with a frost layer 100–150 $\mu$m thick. (This actually represents the total thickness of the combined frost layer of the sphere and brick. The actual layer on the ice sphere is about half this amount.) In Fig. 5 three successive collisions of this frost-ladened sphere with the ice brick are shown. The impact velocity and resulting coefficient of restitution ($\varepsilon$) are also indicated. Note that each successive collision has a lower impact velocity and that the "turnaround" point occurs at a progressively higher point above the hard ice brick surface. This suggests that at low impact velocities the ice sphere has insufficient kinetic energy to compress the frost layer as much as high-velocity impacts. Similar results were observed in other runs.

Note that the second collision has a coefficient of restitution comparable to that of the first impact in spite of

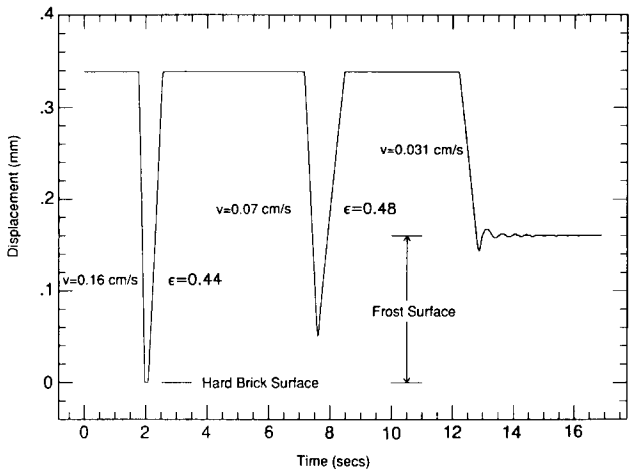


FIG. 5. Output from the CaDD showing the displacement as a function of time for three consecutive collisions of a 2.5-cm radius ice sphere with the ice brick. The sphere and brick have been coated with a frost layer of ~100–150 $\mu$m total thickness. With each successive collision the ice sphere loses its ability to compress the frost layer. The first two impacts are at velocities too high to produce sticking. For the final collision the ice sphere is colliding at just under the critical velocity required for sticking (in this case $v_c \sim 0.03$ cm sec$^{-1}$). Note the damped harmonic motion of the ice sphere just after sticking to the ice brick.

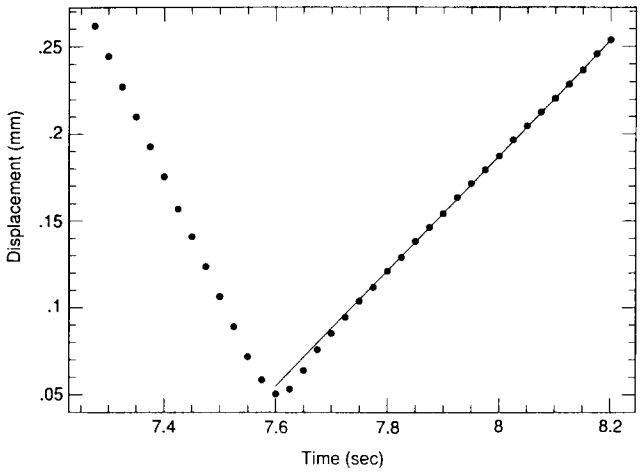


FIG. 6. Close up of the second collision in Fig. 5. In this case the impact velocity is above that required for sticking. After impact the motion of the ice sphere deviates from a constant-velocity motion for the first 50 $\mu$m of the outbound trajectory due to the cohesive force between the two frost layers.

having half the impact velocity (0.07 cm sec$^{-1}$ versus 0.16 cm sec$^{-1}$). But the final collision, which has an impact velocity 0.03 cm sec$^{-1}$, results in the ice sphere bonding to the brick and undergoing a damped harmonic motion prior to coming to a rest on the frost layer. This suggests the existence of a critical impact velocity below which a sticking collision occurs. This was confirmed in subsequent measurements during this experimental run. For impact velocities below about 0.03 cm sec$^{-1}$, a sticking collision *always* occurred. In this run, collisions having an impact velocity above this value *always* resulted in a nonsticking collision but with a much lower coefficient of restitution than that expected for a frost-free ice sphere. In other runs, the critical velocity was sometimes as high as 0.1 sec cm$^{-1}$.

Figure 6 shows an enlarged view of the region around the second collision depicted in Fig. 5. One can see that the cohesive force of the frost layer is having an effect on the motion of the ice sphere even for that collision. Note how on the outgoing trajectory of the ice sphere the cohesive force is decelerating the motion of the ice sphere from a linear motion. Without this decelerating effect, the coefficient of restitution would be ~30% higher. This occurs only while the ice sphere is about 50 $\mu$m from the "contact" point (i.e., the point of maximum compression for the collision). Beyond this point the ice sphere continues with an essentially constant velocity of 0.034 cm sec$^{-1}$.

### *The Spring Constant of Water Frost*

The above results indicate that the contact surface is not a passive region but has dynamical properties. To understand how the surface evolves during a typical sticking collision, we introduce a working model in which the frost layer is treated as a compressible spring. Such dynamical surface properties may determine, in a unified manner, both energy dissipation at moderate and cohesion at low impact velocities.

In Fig. 7 an enlarged view of the cohesive collision of Fig. 5 (third impact) is presented. In this instance the ice

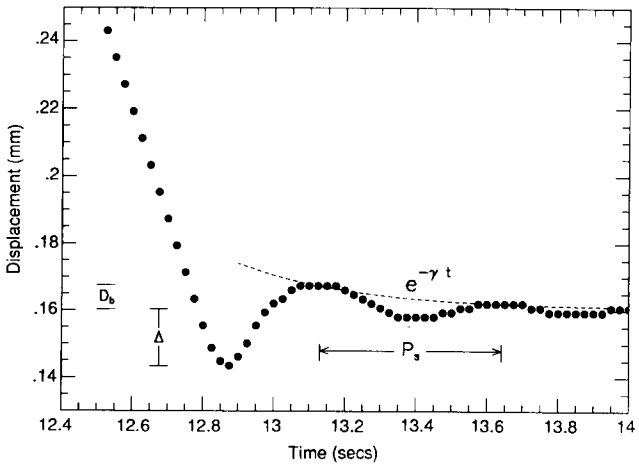


FIG. 7. Close up of the third collision in Fig. 5. In this case the frosted ice sphere is impacting at a velocity below the critical value required for sticking. The ice sphere undergoes a damped harmonic motion with a period, $P_s$, of about 0.5 sec. The quantities Δ and $D_b$ represent the initial amplitude and the range of the force, respectively.

sphere has insufficient kinetic energy after the impact to escape the potential well of the attractive force of the ice layer. It is "trapped" by the surface and undergoes a damped oscillatory motion with a period, $P_s$, of about 0.5 sec before coming to rest approximately 140 $\mu$m above the hard surface of the brick. The maximum amplitude of the oscillations after sticking is about 15 $\mu$m. The oscillations are roughly described by a damped harmonic oscillator and thus suggest a linear force law for the cohesion between the frost-ladened ice particles, which we model using a characteristic "spring" constant $k$. This prescription is a first-order approximation as the period measured using the peak positions decreases slightly with time.

We model the damped harmonic oscillator using four system parameters: the effective spring constant for the frost layer, $k$; the range, $D_b$, over which the attractive force acts (essentially the displacement required to break the cohesive bonds); $\Delta$, the initial amplitude of oscillation; and $\gamma$, the damping coefficient for the oscillations after bonding to the ice brick ($e^{-\gamma t}$). All of these quantities are indicated in Fig. 7. The range of the sticking force can be estimated from Fig. 7 as the distance from the maximum compression point to the maximum amplitude of the ice sphere after the first "bounce" from the hard surface and is about 15 $\mu$m for the collision in Fig. 7. The damping term is obtained from the decay of the maximum amplitude of the harmonic motion of the ice sphere after sticking and is about 2.4 sec$^{-1}$.

The spring constant can be derived from the period of oscillation, $P_s$, of the ice sphere after it has adhered to the ice brick. This period is related to the spring constant by the expression

$$k = \frac{4M_{\text{eff}}\pi^2}{P_s^2} \tag{1}$$

where $M_{\text{eff}}$ is the effective mass of the ice sphere (~475 g) and we have neglected the damping term in the expression for the oscillation frequency. A period of 0.5 sec for $P_s$ corresponds to a value of 7.5 $\times$ 10$^4$ dyn-cm$^{-1}$ for $k$. The slight decrease in period with time indicates some nonlinearity in the restoring force though it may also result from the simple form of the damping term (linear in $v$).

A confirmation that the force law is indeed linear for sticking as well as an independent measure of the spring constant, $k$, could be made by applying a known force, $F$, to the ice sphere after it has adhered to the ice brick. The resulting displacement, $x$, of the ice sphere should vary linearly with the applied force. The slope of this $F - x$ relationship trivially yields the spring constant. The application of such an external force is easily accomplished by allowing a known and steady flow of current to the pendulum solenoid and measuring the displacement

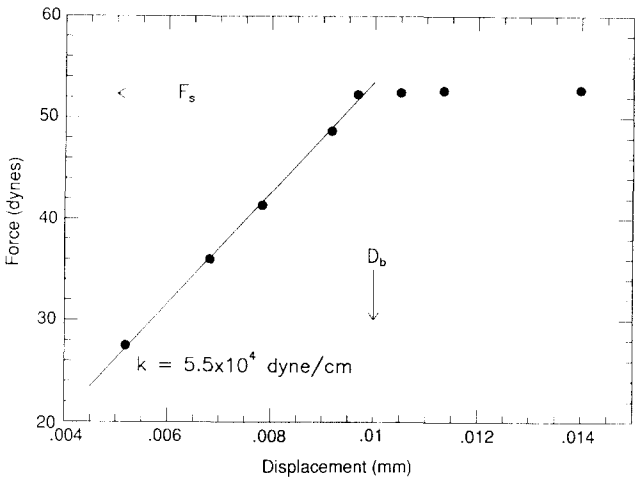


FIG. 8. Displacement of the "stuck" ice sphere as a function of an applied external force for the sticking collision in Fig. 7. The slope of this $F(x)$ relationship yields an independent measure of the spring constant also determined from the oscillatory behavior in Fig. 7. Above a force of 53 dyn the displacement becomes nonlinear, signifying that the cohesive bonds have been broken. This yields a measure of both the sticking force, $F_s$, and the range, $D_b$, of the force.

of the pendulum (and thus ice sphere) via the CaDD as a function of this current.

Figure 8 shows such a $F - x$ relationship measured for the sticking collision depicted in Fig. 7. The response of the ice sphere to this external force is indeed linear and the slope yields a spring constant of the same order of magnitude as derived from the oscillatory behavior in Fig. 7. Note that for an external force greater than about 53 dyn, the displacement becomes nonlinear, signifying that the cohesive bonds have been broken and that the pendulum is now free to oscillate. This gives a measure of both the sticking force, $F_s$, and its range, $D_b$ (displacement required to break the bonds).

The discrepancy between the value of $k$ deduced from Eq. (1) and that from Fig. 8 may be in part attributable to the neglect of the damping term in Eq. (1). In addition, the spring constant measured dynamically may be slightly different than the value obtained from static displacements. During a typical collision, frost particles near the contact region may migrate sideways as well as in the normal direction. In the postcollisional oscillations, the frost particles may move appreciably sideways and in the normal direction and thus significantly modify the spring constant.

Table I summarizes the results of sticking measurements taken with the experimental setup used to acquire the data in Fig. 5. The first two columns give the impact velocity of the sticking collision and the resulting sticking force, respectively. The third column gives the spring constant measured from the slope of the $F - x$ relation-

ship derived from data such as shown in Fig. 8. The column marked $k_{hm}$ represents the value of the spring constant derived from the harmonic motion of the ice sphere after it has stuck to the ice brick (Fig. 7). $D_b$ is the displacement from the stationary position of the stuck ice sphere required to break the cohesive bonds. Finally the last column gives the damping term to the harmonic motion as seen in Fig. 7. Unmeasured quantities are indicated with a dash. The last two entries in the table are measurements taken after colliding the ice sphere with two or three high-velocity impacts ($V_{impact} \sim 0.5$–$1$ cm sec$^{-1}$). The typical errors for the values of the spring constant are 20–30%. In those cases where two independent measurements of the spring constant for the frost layer were made, the two values agreed to within the errors, thus confirming this linear force law for frost cohesion.

Further consistency tests on the veracity of the measured spring constants can be made by considering the sticking force. Assuming that $k$ is independent of the displacement of the ice sphere, the resulting sticking force should be approximately equal to the product of the spring constant and the distance at which the bonds are broken ($kD_b$). Table I yields typical values of $5 \times 10^4$ dyn-cm$^{-1}$ for $k$ and 10 $\mu$m for $D_b$. This results in a sticking force of about 50 dyn, on the order of the typical values measured for the sticking force.

*Dependence on the Frost Thickness*

Several measurements were also taken using an ice sphere of radius 2.5 cm but with a frost thickness of about 10–30 $\mu$m. These are summarized in Table II where we have also tabulated the low-velocity results from an ice sphere with a frost thickness of 100–200 $\mu$m. In this table, we have excluded a few unusually large sticking forces,

TABLE I

**Cohesive Force Measurements: $R_{ball}$ = 2.5 cm, $T$ = 130°K, Frost Thickness ≈ 150 $\mu$m**

| $V_{impact}$ (cm/sec) | $F_s$ (dyn) | $k$ (dyn/cm) | $k_{hm}$ (dyn/cm) | $D_{break}$ ($\mu$m) | $\gamma$ (sec$^{-1}$) |
|---|---|---|---|---|---|
| 0.06 | 30 | — | $1.3 \times 10^5$ | — | — |
| — | 44 | $3.5 \times 10^4$ | | 11 | — |
| 0.015 | 52 | $2.3 \times 10^4$ | $5.7 \times 10^4$ | — | 1.3 |
| 0.031 | 53 | $5.5 \times 10^4$ | $7.5 \times 10^4$ | 10 | 2.4 |
| 0.025 | 45 | $5.1 \times 10^4$ | $4.6 \times 10^4$ | 12 | 2.4 |
| 0.047 | 37 | $1.6 \times 10^4$ | — | 11 | — |
| 0.052 | 30 | — | — | — | — |
| 0.047 | 58 | $7 \times 10^4$ | — | 11 | — |
| 0.049 | 66 | $7 \times 10^4$ | — | 9 | — |
| ... | ... | ... | ... | ... | ... |
| 0.014 | 4 | — | — | — | — |
| 0.056 | 37 | — | — | — | — |

TABLE II

**Cohesive Force Measurements: $R_{ball}$ = 2.5 cm, $T$ = 130°K, $V_{impact} < 0.1$ cm sec$^{-1}$**

| Thickness ($\mu$m) | Mean force (dyn) | Maximum force (dyn) | Minimum force (dyn) |
|---|---|---|---|
| 100–200 | 43 | 62 | 20 |
| 10–30 | 16 | 27 | 11 |

observed in a few cases on the first contact. These values are in the range 100–150 dyn and may represent the maximum sticking force for a typical contact area ~1 mm$^2$. The average sticking force from these measurements as well as the maximum and minimum force measured is tabulated. All measurements were taken at 130°K and with impact velocities prior to sticking of less than 0.1 cm sec$^{-1}$. An increase by an order of magnitude of the frost layer results in an increase in $F_s$ by a factor of only 2 or 3 over the mean sticking force. This lends further support to the hypothesis that the outermost 10–50 $\mu$m of the frost layer is largely responsible for the sticking mechanism.

## V. DISCUSSION

Our sticking measurements indicate that if a sufficiently thick frost layer ($\geq$10 $\mu$m) can be accumulated over the surface of an ice particle, the ability of the particle to adhere to another particle during a collision will be greatly increased. In planetary rings, the abundant micrometer-sized particles (Cuzzi *et al.* 1984) are accreted onto the larger particles, which tends to increase the frost layer thickness, while particle collisions continually pulverize the surface, thereby reducing the thickness of the frost layer (McDonald *et al.* 1989). An ice sphere of radius $R$ moving with a velocity dispersion $v$ with respect to the small particle cloud and orbital angular velocity about the planet, $\Omega$, accretes these grains at a rate of

$$\dot{n}_g \sim \pi R^2 n_g v \sim R^2 \tau_g s^{-2} \Omega \tag{2}$$

where $n_g$, $\tau_g$, and $s$ (~1 $\mu$m) are the number density, optical depth, and size of the grains.

If collisions between particles pulverize all the accreted grains on the surface down to a depth $D_d$, the destruction rate would be

$$\dot{n}_d \sim D_d^2 R s^{-3} \Omega \tau_p \tag{3}$$

where $\tau_p$ is the optical depth of the particles. The critical size above which accretion overcomes destruction is

$$R_{crit} \sim \frac{\tau_p D_d^2}{\tau_g s}. \tag{4}$$

The value of $D_d$ is uncertain. If we utilize the data in Figs. 2 and 3, $D_d$ is unlikely to far exceed a few micrometers since it takes on the order of 10 collisions to pulverize the ~50-$\mu$m frost layer. Voyager data indicate that $\tau_g < 0.1$ for grains of size $10^{-5}$ to $10^{-3}$ (Cuzzi *et al.* 1984). A more recent analysis by Dones (1987), however, indicates that $\tau_g \sim 0.01$. Thus, even in densely populated regions of Saturn where $\tau_p \sim 1$, $R_{crit}$ is comparable or much smaller than typical centimeter-sized particles so that most ring particles are expected to be coated with a frost layer. If we assume $D_d$ is a significant fraction of the frost layer, the minimum thickness of the frost layer would be $\sim(Rs\tau_g/\tau_p)^{1/2} \sim 10$–$100$ $\mu$m which is comparable to the thickness of the layer in our experiments.

The data in Fig. 5 indicate that there is a critical impact velocity above which sticking can no longer occur. For velocity less than 0.03 to 0.1 cm sec$^{-1}$ the collisions are cohesive. Since the velocity dispersion in Saturn's ring is estimated to be in this range, it may be possible that collisions among particles result in cohesion in some parts of the rings.

*Composite Particles*

After a cohesive collision between two particles with comparable radius, the gravity between them is $\sim G\rho^2R^4$ where $\rho$ (~1 g cm$^{-3}$) is the mass density of the particles. The data in Figs. 2 and 3 and Table I imply that the sticking force is greater than gravity for all but the largest meter-sized particles in planetary rings. Collisions could lead to coagulated clusters of particles. In this case, the sticking strength of the cluster is increased by the number of contact surfaces between constituent particles which enhances the dominance of sticking force over gravity. Thus, dynamical ephemeral bodies (Greenberg *et al.* 1983, Weidenschilling *et al.* 1984), if they exist, are more likely to be bound by sticking force than by gravity.

Using the magnitude of the sticking force for water frost, $F_s$, determined in our experiments, the size of conglomerate particles can be estimated under various assumptions. For the following rough calculations we take $F_s \approx 100$ dyn and assume a contact area of order 1 mm$^2$. For thicker frost layers and/or particles with larger radii, the contact area could well be enlarged. Consequently, without any information on the thickness of the frost layer, our calculations only give the order-of-magnitude determination on the limiting particle size for which Saturnian gravitational tidal forces or impulsive impact forces are comparable to $F_s$. The tidal force, $F_T$ between two equal masses, $m_p$, separated by a distance $\Delta r$ is $F_T \approx 2m_p\Omega^2\Delta r$, where $\Omega$ is the angular frequency of an orbiting particle ($\approx 1.75 \times 10^{-4}$ rad sec$^{-1}$). Two situations are considered: a chain of particles and a rough spherical aggregate of small particles. For the limiting case of two equal particles in a chain, the size limit is set by ($\Delta r \approx 2r$)

$$F_s \approx 8/3\rho\pi r^3\Omega^2(2r) \tag{5}$$

$$r = (3F_s/16\pi\rho\Omega^2)^{1/4} \approx 120 \text{ cm} \tag{6}$$

where $\rho = 1$ g cm$^{-3}$.

For smaller-sized particles larger chains are stable against the tidal forces. For example, for particles of radius 50 cm ($m_p \approx 5. \times 10^5$ g), the length of a stable chain would be $L = F_s/2m_p\Omega^2 \approx 30$ m, and smaller particles would form yet longer chains. However, because the probability of forming a long chain is small and the likelihood of breaking a chain via impact forces is high as discussed below, chains of more than a few particles will not exist in dynamical equilibrium.

For spherical aggregates of radius $r$ formed of particles of diameter $d$ we consider the case where tidal forces split the aggregate into two equal halves. In this case the effective sticking force across the fracture plane is $NF_s$ where $N$, the number of contacts, is approximately $\pi r^2/d^2$. Then

$$F_s\pi r^2/d^2 \approx (4\rho/3)\pi r^4\Omega^2. \tag{7}$$

We obtain

$$r \sim \left[\frac{F_s}{\rho d^2\Omega^2}\right]^{1/2}. \tag{8}$$

For $d = 10$ cm, $r = 70$ m, and for meter-sized spheres the composite radius would be $r = 6$ m. For these large particles, the gravity becomes an important binding force.

Since the largest sticking forces measured for small particles are of the order of 100 dyn, we view these estimates as upper limits to the size of composite objects formed of small (<5-cm) particles. In particular, the size of spherical aggregates will likely be smaller since a range of contact sticking forces would be expected. Thus from tidal force considerations we think that composite particles held together by contact sticking forces are generally less than 10 m in radius. This gives a value in the same range as the largest abundant particles in Saturn's rings observed by the Voyager Radio occultation (Marouf *et al.* 1983).

*Impact Forces*

Our measurements of the coefficient of restitution for frosted ice particles indicated that the impact time for collisions is about 0.1 sec or less. The impact force, $F_I$, can thus be estimated if we assume the momentum change in a collision is comparable to the relative momentum of the lighter particle. Thus

$$F_I = mv/\tau. \tag{9}$$

For a 10-cm-diameter sphere moving at a dispersion velocity of 0.1 cm $sec^{-1}$ and a collision time of 0.1 sec, the impulsive force is large (~500 dyn). Shorter collision times and/or larger particles yield even larger impulsive collision forces. To separate two particles held together via sticking forces we must consider the component of $F_I$ along the sticking bond. For composite particles the fraction of collisions for which $F_I$ would separate the particles is less than $\frac{1}{4}$. Even then the impact forces are still very large compared to the measured sticking forces. Thus, unless collisions can be softened by thick layers of frost (i.e., larger $\tau$) or the sticking forces are appreciably stronger than the values to date, the size of the aggregates will be severely constrained to clusters of at most a few particles. The limitations imposed by the magnitude of the impulsive impact forces appear far more important for Saturn's rings than the tidal forces.

When one considers impact forces it readily becomes apparent why there is a critical impact velocity below which a collision always results in the cohesion of two particles. For a particle to stick the cohesive forces must be greater than the impulsive force of the collision. Thus

$$v_{crit} \approx F_s \tau / M_{eff} \quad (10)$$

where $\tau$ is the collision time, $M_{eff}$ is the effective mass of the ice sphere, and $F_s$ is the largest measured sticking force. The data in Table I yield $F_s = 66$ dyn. Figure 6 indicates that $\tau \sim 0.1$ sec and the effective mass of the ice sphere is 400 g. This yields a critical velocity of 0.025 cm $sec^{-1}$, very near the measured value of 0.03 cm $sec^{-1}$ for the data presented in Table I.

## VI. SUMMARY

The sticking measurements presented here represent the first such of their kind. Further measurements are needed to establish the dependence of the sticking force on the frost layer thickness. The sticking force may also vary with the collisional contact area, necessitating the need for measurements using ice spheres having a different radius of curvature. Our measurements indicate that the sticking force is maximized for intermediate collisional velocities and that the very low (0.01 cm $sec^{-1}$) and very high (1 cm $sec^{-1}$) impact velocities result in negligible sticking forces. It is important to try to determine some functional form for this velocity dependence. Finally, these measurements were made using only water ice. Clearly the cohesive force of different types of ices should be measured as they are likely to be present in the Saturn ring environment.

## ACKNOWLEDGMENTS

We thank J. McDonald for his assistance in performing some of the experiments and for useful discussions. This work was supported by NASA Grant NAGW-590. This work is Lick Observatory Contribution No. 464.

## REFERENCES

BORDERIES, N., P. GOLDREICH, AND S. TREMAINE 1984. Unsolved problems in planetary ring dynamics. In *Planetary Rings* (R. Greenberg and A. Brahic, Eds.), pp. 713–734. Univ. of Arizona Press, Tucson.

BRIDGES, F., A. HATZES, AND D. LIN 1984. Structure, stability, and evolution of Saturn's rings. *Nature* **309,** 333–335.

CUZZI, J. N., J. J. LISSAUER, L. W. ESPOSITO, J. B. HOLBERG, E. A. MAROUF, G. L. TYLER, AND A. BOISCHOT 1984. Saturn's rings: Properties and processes. In *Planetary Rings* (R. Greenberg and A. Brahic, Eds.), pp. 73–199. Univ. of Arizona Press, Tucson.

CUZZI, J. H., J. B. POLLACK, AND A. L. SUMMERS 1980. Saturn's rings: Particles, composition, and size distribution as constrained by observations at microwave wavelengths. II. Radio interferometric observations. *Icarus* **44,** 683–705.

DONES, L. 1987. Ph.D. thesis, University of California, Berkeley.

GOLDREICH, P., AND S. TREMAINE 1978. The velocity dispersion in Saturn's ring. *Icarus* **34,** 227–239.

GREENBERG, R., D. R. DAVIS, S. J. WEIDENSCHILLING, AND C. R. CHAPMAN 1983. *Bull. Amer. Astron. Soc.* **15,** 812.

HATZES, A. P., F. G. BRIDGES, AND D. N. C. LIN 1988. Collisional properties of ice spheres at low impact velocities. *Mon. Not. R. Astron. Soc.* **213,** 1091–1116.

JEFFREYS, H. 1947. The effects of collisions on Saturn's rings. *Mon. Not. R. Astron. Soc.* **107,** 263.

MAROUF, E. A., G. L. TAYLER, H. A. ZEBKER, AND V. R. ESHLEMAN 1983. Particle size distributions in Saturn's rings from Voyager I radio occultation. *Icarus* **54,** 189.

MAXWELL, J. C. 1859. *On the Stability of the Motion of Saturn's Rings.* MacMillan, Cambridge/London.

MCDONALD, J. S. B., A. HATZES, F. BRIDGES, AND D. N. C. LIN 1989. Mass transfer during ice particle collisions in planetary rings. *Icarus* **82,** 167–179.

PILCHER, C., C. R. CHAPMAN, L. A. LEBOFSKY, H. H. KIEFFER 1970. Saturn's rings: Identification of water frost. *Science* **167,** 1372–1373.

WEIDENSHILLING, S. J., C. R. CHAPMAN, D. R. DAVIS, AND R. GREENBERG 1984. Ring particles: Collective interactions and physical nature. In *Planetary Rings* (R. Greenberg and A. Brahic, Eds.), pp. 367–415. Univ. of Arizona Press, Tucson.